processes

Article

Study on the Evolution Law of Inclusions in the Whole Process and Evaluation of Cleanliness in Start and End of Casting Billets of 42CrMo-S Steel

Lidong Xing [1,2], Bo Wang [1], Yanping Bao [1,*] and Min Wang [1,2]

[1] State Key Laboratory of Advanced Metallurgy, University of Science and Technology Beijing (USTB), Beijing 100083, China
[2] Technical Support Center for Prevention and Control of Disastrous Accidents in Metal Smelting, University of Science and Technology Beijing (USTB), Beijing 100083, China
* Correspondence: yanping_bao@163.com

Abstract: To investigate the evolution law of inclusions in 42CrMo-S steel, this paper samples and analyzes the steel during its refining process as well as the head and tail billets. An oxygen and nitrogen analyzer, a scanning electron microscope (SEM) equipped with energy-dispersive X-ray spectrometry (EDS), and an ASPEX automatic inclusion scanning electron microscope are employed to analyze the cleanliness level of the molten steel in the refining stage and the head and tail billets. The results demonstrate that the total oxygen content at the end of LF slagging is 10.2 ppm, indicating that the refining slag has an excellent deoxygenation effect. During the RH refining process, the total oxygen content of the molten steel diminishes to less than 10 ppm and reaches 6.3 ppm at end-RH. The nitrogen content in the molten steel gradually increases during the smelting process and attains 65 ppm at end-RH. Upon arrival at LF, pure Al_2O_3 plays the role of the primary inclusions in the molten steel. Afterwards, the pure Al_2O_3 inclusions transform into Mg-Al spinel-type inclusions, Al_2O_3-MgO-CaO inclusions, and Al_2O_3-CaO inclusions. The number of CaS-type inclusions in the steel reaches the maximum after feeding the S wire. In the RH refining stage, the percentage of inclusions with a size less than 5 μm is maintained above 90%. Finally, the cleanliness level of the head and tail billets (the start and end of a casting sequence) is analyzed, and it is recommended that the cut scrap length for the head billet is 0.3 m and the reasonable cutting scrap length for the tail billet is 1 m.

Keywords: 42CrMo-S; evolution of inclusions; content of oxygen and nitrogen; head billets; tail billets; cut scrap length

Citation: Xing, L.; Wang, B.; Bao, Y.; Wang, M. Study on the Evolution Law of Inclusions in the Whole Process and Evaluation of Cleanliness in Start and End of Casting Billets of 42CrMo-S Steel. *Processes* **2023**, *11*, 2184. https://doi.org/10.3390/pr11072184

Academic Editor: Jun Zhang

Received: 2 July 2023
Revised: 18 July 2023
Accepted: 20 July 2023
Published: 21 July 2023

1. Introduction

42CrMo-S steel is extensively utilized because of its superior hardenability, higher strength and toughness, excellent impact resistance and fatigue properties after tempering, and outstanding impulse toughness at low temperatures [1–4]. Currently, Cr-Mo series gear steels are mainly used in construction machinery, aviation generators [5–7], and some structural components (crankshafts, bearings, and bolts) [8–11]. The cleanliness of steel is a crucial indication of the overall quality level of steel and affects its performance [12–14]. The cleanliness level of the steel can be evaluated via the morphology, quantity, size, and distribution of non-metallic inclusions in the steel [15–20]. Hence, studying the evolution of inclusions for the whole process in the steel is a necessary way to control the cleanliness of steel.

The type of inclusions in Al-killed steel are mainly Al_2O_3, Al_2O_3-MgO, Al_2O_3-SiO_2, etc. Al_2O_3-type inclusions have high melting points and tend to cause clogging of SENs, which in turn affects the property of the steel [21]. For this reason, researchers have tried to reduce the detriment by changing the phase equilibrium of non-metallic inclusions [22] and controlling the basicity of the refining slag [23]. In addition, calcium treatment is also frequently applied in the control of inclusions in Al-killed steel since calcium treatment can modify clustered Al_2O_3 inclusions into low-melting point calcium aluminate inclusions [24–26], which facilitates the upward removal of inclusions and improves the steel quality. However, Ca wires fed into sulfur-containing steel will react with the sulfur to form CaS, which causes clogging of SENs [27]. Therefore, it is imperative to elucidate the whole process evolution of inclusions in Al-killed sulfur-containing steel.

Although there has been a long history of research on inclusions, there are still fewer investigations on the cut scrap length of head and tail billets. A reasonable cut scrap length can reduce unnecessary scrap and guarantee product quality [28,29]. Excessively, the long-cut waste length will raise production costs and impose economic losses. Too-short-cut scrap lengths will not only affect the quality of the cast billets and deteriorate the property of the steel, but also lead to the inability of the crane clamps to hold the waste billets. Therefore, it is desirable to discuss the cleanliness of the head and tail billets and propose a reasonable cut scrap length.

Based on this, actual 42CrMo-S steel produced in a mill is employed as the investigation target in this study. Samples are taken from the molten steel in its refining stage to analyze the law of oxygen and nitrogen variation and the rule of inclusion type, quantity, size, distribution, and morphology. In addition, the cleanliness level of the head and tail billets is analyzed to explore the discrepancy against the normal billets. So, a reasonable length for cutting scrap is proposed to guide further advancement in product quality and reduce production costs.

2. Experimental Materials and Methods

2.1. Experimental Material

The experimental material studied in this paper is derived from 42CrMo-S steel produced by a steel mill, whose smelting process is "150 t top-bottom blowing converter→LF refining→RH refining→48 t large-capacity T-type tundish→bloom continuous casting". The specific technological process is shown in Figure 1. Beginning with the addition of alloy to the ladle when the tapping of the converter reaches 1/4, lime and pre-molten slag are added into the LF feeding station to make white slag and aluminum chips is added in small amounts within the multiple batches. After the LF refining stage is finished, the Ca wires are fed about 150 m. The S wire is fed before leaving the station, and the interval between S wire and Ca wire feeding is not less than 5 min. In the RH refining process, the argon is bottom-blown throughout the entire process for more than 45 min, and the vacuum time is kept above 12 min. The sulfur and aluminum contents are adjusted according to the actual situation after breaking the vacuum of RH to maintain the soft blowing time as more than 15 min before leaving the station of RH. The composition control requirement of 42CrMo-S is shown in Table 1.

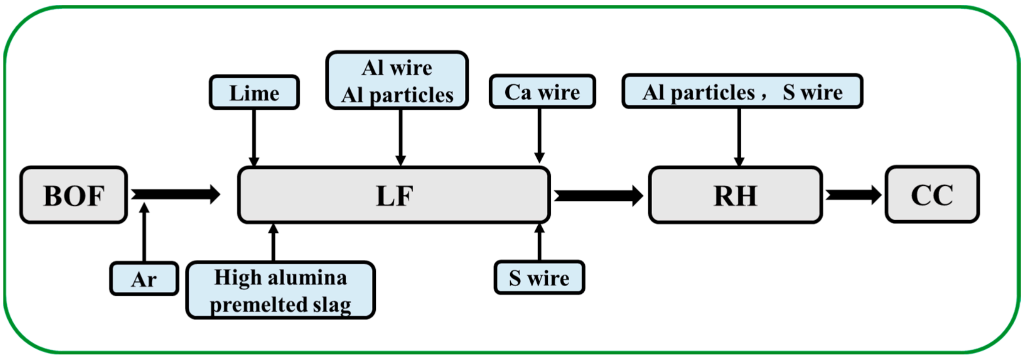

Figure 1. 42CrMo-S smelting process.

Table 1. 42CrMo-S composition control requirement (wt.%).

	C	Si	Mn	P	S	Cr	Mo
Internal control	0.40–0.42	0.26–0.33	0.75–0.80	≤0.015	0.017–0.030	1.11–1.16	0.17–0.20
Target	0.41	0.27	0.77	≤0.010	0.020	1.13	0.18

2.2. Experimental Methods

Performed separately in the LF arrival station, high basicity slag formation, Ca wire feeding, S wire feeding, RH arrival station, and the breaking vacuum of RH and end-RH occur in order to extract the bucket sample. The cake sample in the tundish is taken and a full section bloom sample in continuous casting bloom is collected. The specific sampling plan and sample numbers are shown in Table 2.

Table 2. Sample plan of 42CrMo-S.

Sampling Time	Sample Number
Arrival to LF	L1
LF high basicity slag formation	L2
3 min after feeding the Ca wire	L3
3 min after feeding the S wire	L4
Arrival to RH	R1
Break vacuum of RH	R2
End-RH	R3
20 min of tundish	C1

The sampling method for the head billet is shown in Figure 2a. The casting temperature is 1520 °C and the casting speed is 0.55 m/min. The electric stirring parameter is 200 A 2.5 Hz, and the mold water volume is 3800 L/min. The water ratio is 0.2 L/kg. The sampling length is 500 mm, and a low-frequency sample is cut every 100 mm. The first cut sample is defined as T1, and the last cut sample is described as T5. Similarly, the sampling method for the tail billet is shown in Figure 2b. The sampling length is 3000 mm, and the first cut sample is defined as W1 (1000 mm from the tail). Then, a low-fold sample is cut every 500 mm, and the last cut sample is described as W5.

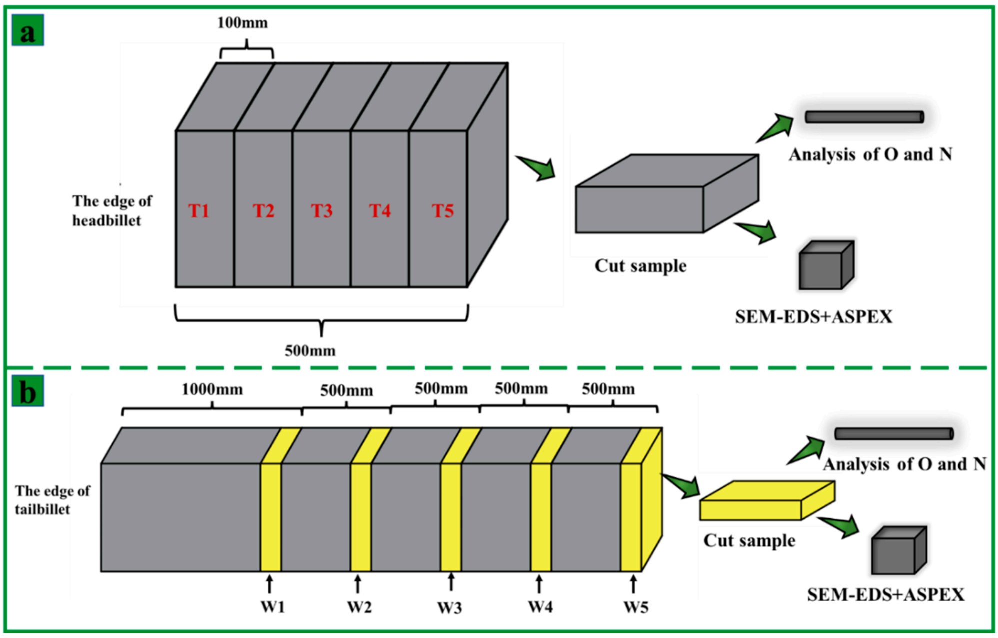

Figure 2. (**a**) Head billet sampling plan and (**b**) tail billet sampling plan.

The metallographic specimen is taken out at the center of the wide surface of the head and tail billets from 1/2 of the inner arc for an automatic scanning of inclusions to analyze the variation law of inclusions type, quantity, and size. At the same time, the oxygen and nitrogen rods are extracted around the metallographic specimen to analyze the variation of the oxygen and nitrogen content in the head and tail billets.

The size of the oxygen and nitrogen rods is Φ 5 × 7 mm. In this paper, the oxygen and nitrogen content of the samples is determined using a high-frequency infrared oxygen–nitrogen analyzer. The oxygen and nitrogen rods are cleaned with alcohol, dried, and then put into the graphite crucible. After weighing the weight, the graphite crucible, which the sample is added into, is placed in the machine. Then, the analyzer is run to obtain the content of the oxygen and nitrogen.

The size of the cut metallographic sample is 10 × 10 × 10 mm (Figure 2). These metallographic samples are embedded with a thermal automatic setting machine, and the setting powder is made of acrylic resin. The sample is ground and polished using an automatic polishing machine and an automatic ground machine after embedding. After completing the above work, the prepared sample can be used for the next detection.

An automatic scanning of inclusions requires a higher surface quality of samples. The surface of the embedded metallographic sample is cleaned and affixed with conductive adhesive and aluminum foil. The samples are then placed in the ASPEX automatic inclusion scanning electron microscope and the number of inclusions of different types and sizes can be obtained.

3. Study of the Cleanliness Level in the Whole Process

3.1. Variation of Oxygen and Nitrogen in the Whole Process

The variation in the oxygen and nitrogen content in the whole refining process of 42CrMo-S is shown in Figure 3. The total oxygen content at arrival to LF is 60.2 ppm. In the LF station, high basicity slag is formed, and the total oxygen content decreases to 10.2 ppm. The huge degree of reduction in the oxygen content shows that LF refining has a brilliant deoxidation effect. The total oxygen content increases by 4 ppm after feeding the Ca and S wires and increases by 3 ppm at the arrival to RH, which indicates that a secondary oxidation phenomenon occurs during this period. RH refining reduces the total oxygen content to less than 10 ppm, and the total oxygen content is 6.3 ppm at end-RH. However, the oxygen content of the molten steel increases in the tundish, indicating that the phenomenon of secondary oxidation exists at this period. So, the casting should be reasonably protected. The total oxygen content in the rolled steel is 7.2 ppm, which is lower than the internal control requirement of 15 ppm.

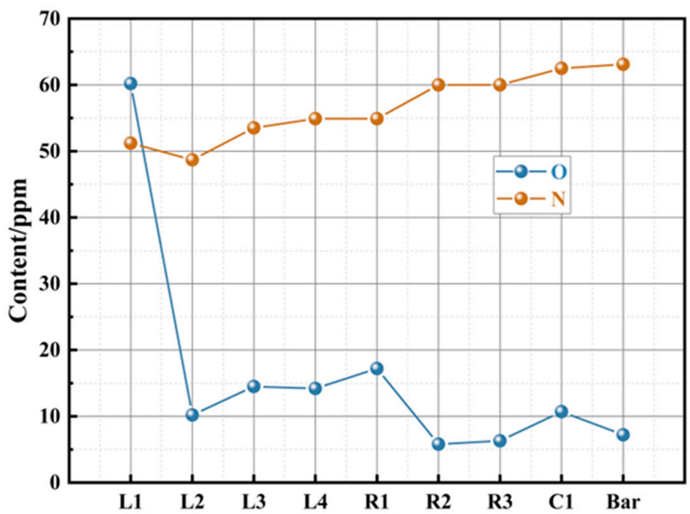

Figure 3. Analysis of oxygen and nitrogen in the whole process of 42CrMo-S.

Overall, the whole refining process has been effective in controlling the total oxygen content in the steel. However, the nitrogen content in the molten steel shows a gradual improvement trend during the refining process. The nitrogen content has the largest number of 62.5 ppm in the tundish. A violent reaction of the molten steel when the Ca wire is fed and inhalation of air from the exposed steel surface is experienced is why the nitrogen content increases in the LF refining stage. The nitrogen content does not show a reduction trend during the RH refining process, suggesting that the RH vacuum treatment in this heat is not effective at denitrifying the molten steel. The content of nitrogen at end-RH and rolling stock is greater than 60 ppm, which is higher than 55 ppm of the internal control requirement. Therefore, it is necessary to focus on the control of the nitrogen content in the steel in other heats.

3.2. The Evolution of Inclusions in the Whole Process

The variation in the number and type of inclusions in the 42CrMo-S is shown in Figure 4. The number of inclusions decreases as the refining process proceeds, where the lowest number of inclusions is recorded at the end of LF slagging (Figure 4a). After feeding Ca wire, Al_2O_3-CaO-type inclusions and CaS-containing inclusions are generated, and the number of inclusions increases. The number of inclusions gradually decreases during the RH refining stage, indicating that RH refining has a brilliant inclusion removal capacity. Variation in the inclusions type is shown in Figure 4b,c. The inclusions in the molten steel upon arrival at LF are mainly pure Al_2O_3 inclusions and minor Al_2O_3-SiO_2 inclusions. The number of pure Al_2O_3 inclusions gradually diminishes with the refining process proceeds and is modified into Mg-Al spinel-type inclusions, Al_2O_3-MgO-CaO composite inclusions, and Al_2O_3-CaO inclusions. Before L4 (feeding the S wire) occurs, inclusions in the molten steel are dominated by Al_2O_3-type inclusions. Starting from L4 (feeding the S wire), there is a significant increase in the number of CaS-type inclusions in the molten steel. Types of inclusions no longer fluctuate during the RH refining process. There is almost no change in the number of Al_2O_3-SiO_2 inclusions throughout the whole smelting process. The proportion of different types of inclusions is shown in Figure 4d. The S wires are fed into the molten steel, where the proportion of CaS inclusions is the largest. The proportion of pure Al_2O_3 inclusions also increases, indicating the existence of secondary oxidation at this period. The number of Al_2O_3-SiO_2 inclusions primarily decreases and then increases as the refining process proceeds.

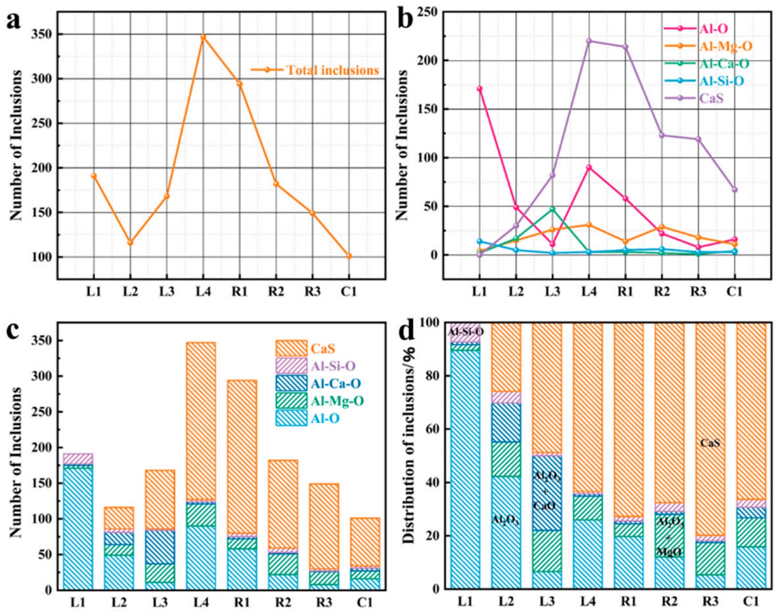

Figure 4. (**a**) The variation in total number of inclusions and (**b**,**c**) inclusions type and (**d**) the proportion of different types of inclusions.

The distribution of inclusions of different sizes during the refining process is shown in Figure 5. The inclusions are closely distributed during arrival to LF, S wire feeding, arrival to RH, and end-RH. The inclusions are more diffusely distributed during high basicity slag formation; Ca wire feeding; breaking of the vacuum; and arrival to RH, end-RH, and the tundish stages. The diminutive inclusions gather obviously during arrival to RH, and large-size inclusions decrease significantly from end-RH to the tundish. The distribution of inclusions in LF high basicity slag formation is consistent with the results of the oxygen and nitrogen analysis above.

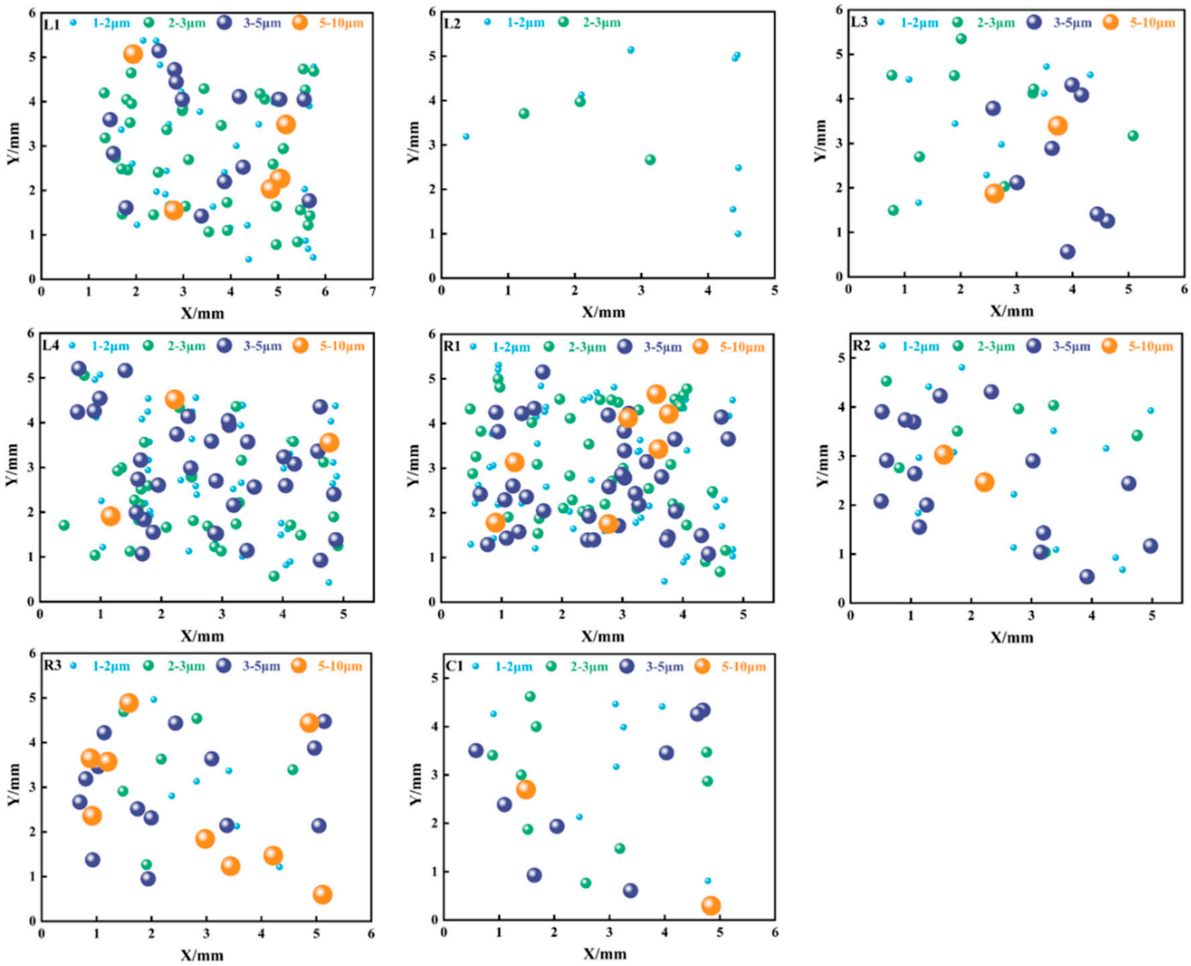

Figure 5. The distribution of inclusions in different sizes in different process stages.

The variation in the number of inclusions in different sizes for the whole process of 42CrMo-S is shown in Figure 6. Variation in the inclusions size in the refining process is shown in Figure 6a,b. The number of inclusions whose sizes are less than 5 μm decreases and then increases as the refining process proceeds, as well as reduces again in RH refining. The number of inclusions whose sizes are larger than 5 μm does not fluctuate much. The distribution of size in inclusions is performed in Figure 6c. The inclusions between 1 and 4 μm account for the vast majority in the refining stage. It is obvious that the distribution of inclusions is more intensive in feeding the S wire and arrival to RH, which is consistent with the above analysis. The proportion of inclusions in different sizes is shown in Figure 6d. The proportion of inclusions smaller than 5 μm is more than 90% in LF refining. The proportion of inclusions larger than 5 μm is the largest at end-RH, which means that RH refining can make inclusions gather and float to remove and enhance the cleanliness level of the molten steel.

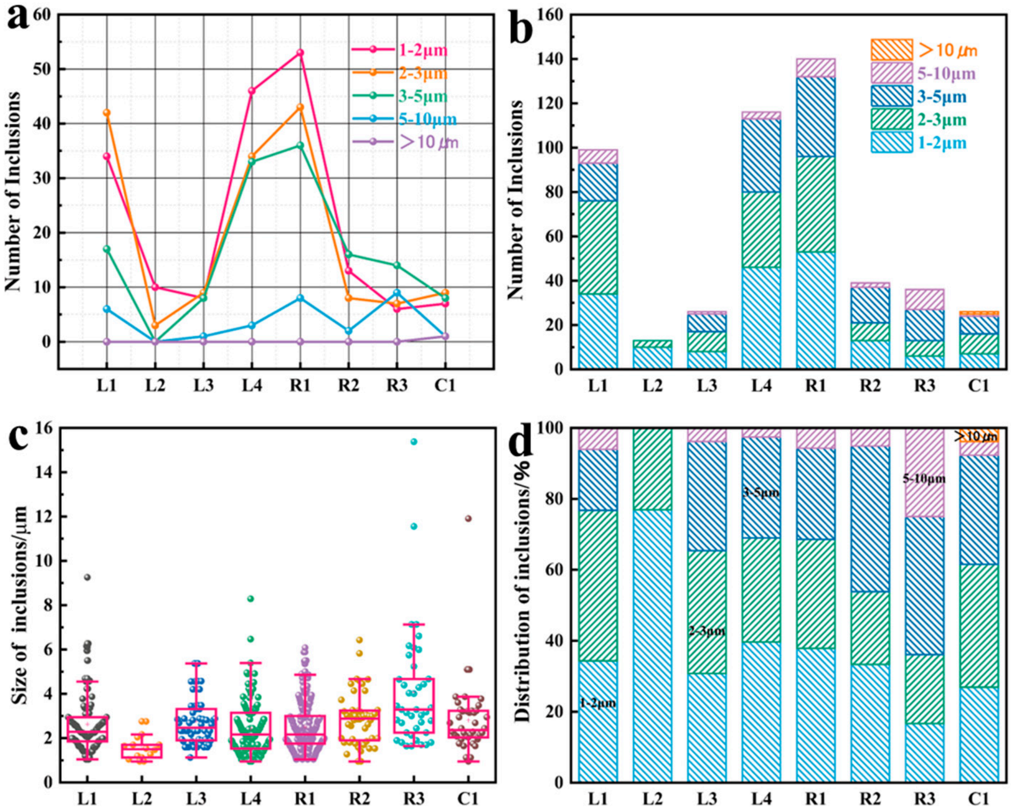

Figure 6. (**a**,**b**) The variation in inclusions size, (**c**) the distribution of inclusions size in different process stages, and (**d**) the proportion of different sizes of inclusions.

In general, the size of inclusions in the refining process tends to increase. However, the percentage of inclusions which are smaller than 5 μm in the refining process (except end-RH) is kept above 90%. Almost no inclusions are larger than 10 μm in the whole refining process, which means that the refining process controls the large inclusions well. However, very few inclusions larger than 10 μm are detected in the tundish, which might be due to the large inclusions that are formed by the aggregation of the RH refining process and are not removed by floating.

4. Study on the Reasonable Cutting Scrap Length

4.1. Head Billet

4.1.1. Analysis of Oxygen and Nitrogen Content

The results of the oxygen and nitrogen content testing of the head billet are shown in Figure 7. The blue arrow indicates that the blue curve (oxygen content) corresponds to the left axis, and the yellow arrow indicates that the yellow curve (nitrogen content) corresponds to the right axis. The nitrogen content of the head billet does not fluctuate much with the growth in casting length. T5 has the largest nitrogen content of 68.2 ppm among the five cut samples, which is lower than 70 ppm in the normal billet. The oxygen content of the head billet shows a descending trend with the growth in casting length but is still higher than 11.7 ppm of the normal billet. The oxygen content decreases from 21.1 ppm to 15.2 ppm during T2 to T3 and then stabilizes at around 15 ppm from T3 to T5. Therefore, based on the oxygen and nitrogen detection, the reasonable cut scrap length for the head billet is not less than 0.3 m.

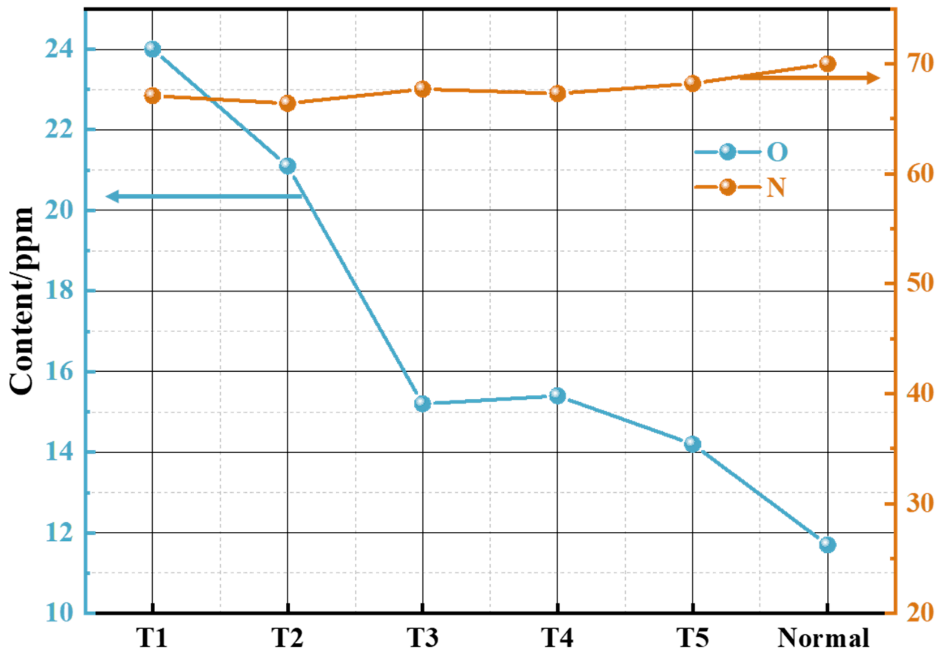

Figure 7. Analysis of oxygen and nitrogen content of the head billet.

4.1.2. The Evolution of Inclusions of the Head Billet

The variation in the total number of inclusions in various positions of the head billet is shown in Figure 8a. The total number of inclusions in the head billet decreases from 236 to about 100 with the growth of casting length. The normal billet is obtained when continuous casting is in stable production and the number of inclusions in the normal billet is 150, which is closest to the number of inclusions in T3. The variation in the type of inclusions in the 42CrMo-S head billet is shown in Figure 8b. The number of pure Al_2O_3 inclusions and Al_2O_3-SiO_2 inclusions reduces most obviously. In addition, the number of pure Al_2O_3 inclusions and Al_2O_3-MgO inclusions in the head billet is higher than those in the normal billet. The reason why the inclusion level in T5 is much lower than the normal billet is that T5 has fewer Al-Si-O-type inclusions. The Al-Si-O-type inclusions are mainly introduced by the capping agent, which indicates that the tundish is better protected at T3–T5, making it have fewer Al-Si-O-type inclusions than the normal billet.

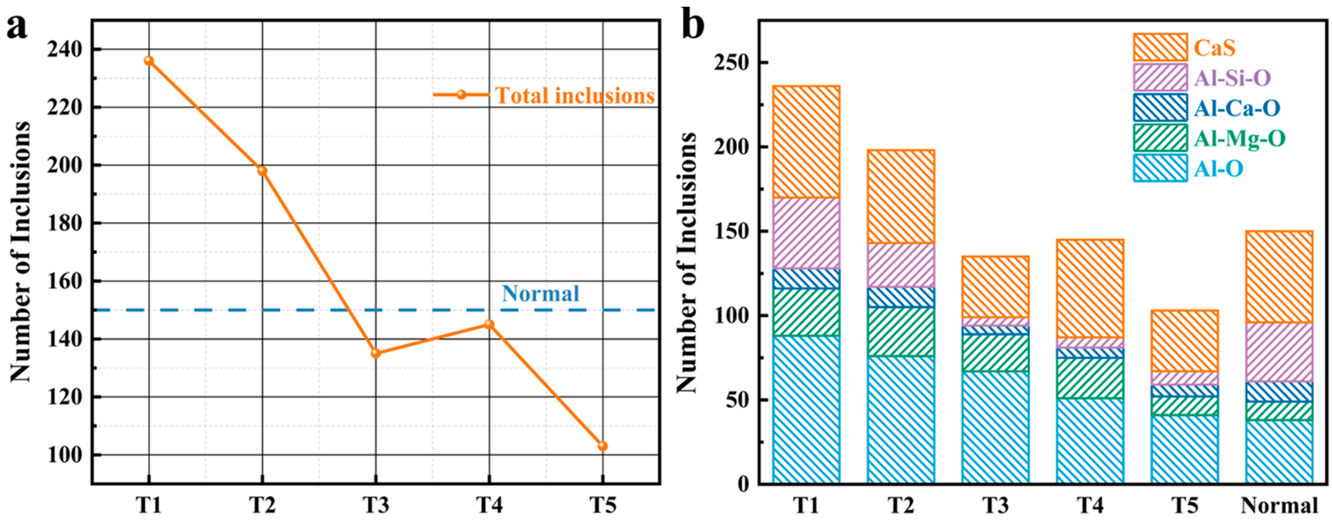

Figure 8. The variation in (**a**) total inclusions and (**b**) inclusions type.

In summary, the reasonable cut scrap length of the head billet is 0.3 m.

4.2. Tail Billet

4.2.1. Analysis of the Oxygen and Nitrogen Content

The results of the oxygen and nitrogen content testing of the tail billet are shown in Figure 9. The blue arrow indicates that the blue curve (oxygen content) corresponds to the left axis, and the yellow arrow indicates that the yellow curve (nitrogen content) corresponds to the right axis. The nitrogen content performs a descending trend from W1 to W5. The nitrogen content of W5 is 48 ppm, which is the smallest among the five cut samples but still higher than 40.4 ppm of the normal billet. The total oxygen content of the tail billet does not vary much with the growth of casting length and is stable at about 15 ppm, which is higher than 10.8 ppm of the normal billet. However, the oxygen content of the tail billet meets the internal control requirements, so W1 can be used as the normal billet.

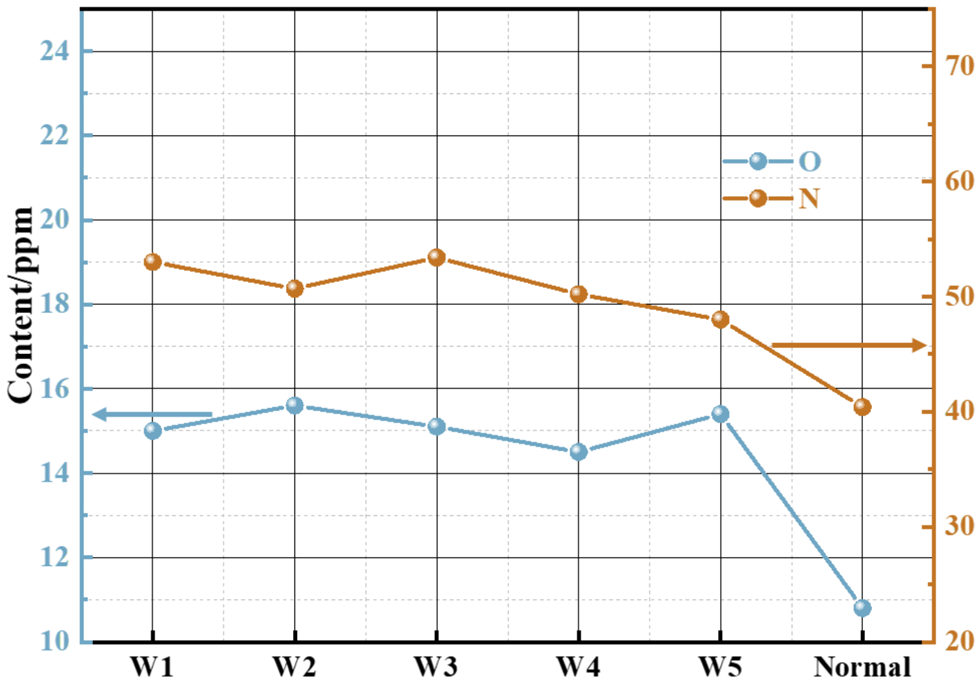

Figure 9. Analysis of oxygen and nitrogen content of the tail billet.

It can be obtained from Figures 7 and 9 that the oxygen and nitrogen content of the tail billet is lower compared to the head billet. The oxygen content reflects the amount of small-sized oxidized inclusions in the cast billet, and the nitrogen content reflects the degree of secondary oxidation of the molten steel. Therefore, the cleanliness level of the tail billet is higher than the head billet.

4.2.2. The Evolution of Inclusions in the Tail Billet

The variation in the total number of inclusions in various positions of the tail billet is shown in Figure 10a. The total number of inclusions in the tail billet primarily declines and then increases with the growth of casting length. The number of inclusions in the normal billet is 86. W2 has the least number of inclusions, and W4 and W5 have the same number of inclusions. Incidentally, the number of inclusions at W1 is 95, which is closest to the normal billet.

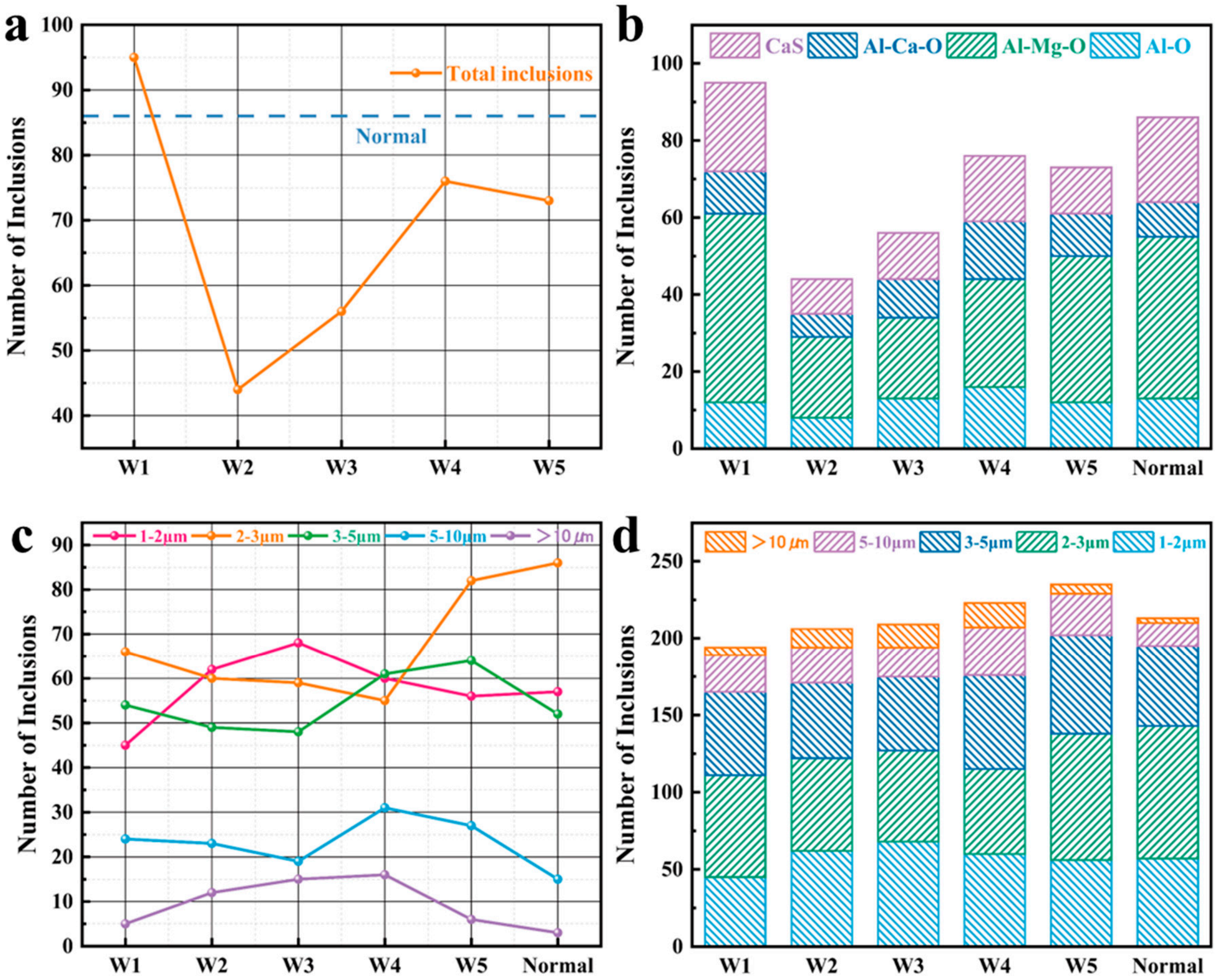

Figure 10. The variation in (**a**) total inclusions, (**b**) inclusion types, and (**c**,**d**) inclusion sizes.

The variation in the number of different types of inclusions in the 42CrMo-S tail billet is shown in Figure 10b. Compared with the normal billet, the overall number of inclusions in the tail billet is slightly lower, but the types of inclusions are consistent with the normal billet. The number of Al_2O_3-CaO inclusions and Al_2O_3-MgO inclusions in the tail billet is obviously higher than the normal billet. The amount of pure Al_2O_3 inclusions, Al_2O_3-MgO inclusions, and Al_2O_3-CaO inclusions at W1 is almost the same as the normal billet. The variation in inclusion sizes is shown in Figure 10c,d. Compared with the normal billet, the size of oxide inclusions in the tail billet is mainly 1–5 μm, and the difference against the normal billet is not significant. The number of inclusions whose sizes are larger than 5 μm in the tail billet is slightly higher than that in the normal billet, where the number of inclusions of different sizes in W1 is closest to that in the normal billet.

In summary, the reasonable cut scrap length of the tail billet is 1 m.

4.3. Morphology and Size Distribution of Inclusions in the Head and Tail Billets

The reasonable cut scrap length of the head and tail billets is obtained above using an oxygen and nitrogen analysis and a cleanliness investigation. It is found that the types of inclusions in the head billet and tail billet do not differ much from Figures 8b and 10b. The morphology and map scan results of typical Al_2O_3-MgO-CaO-CaS inclusions and Al_2O_3-CaO-MgO inclusions are shown in Figure 11. The morphology and energy spectrum of Al_2O_3-MgO-CaO-CaS inclusions and MnS inclusions are shown in Figure 12.

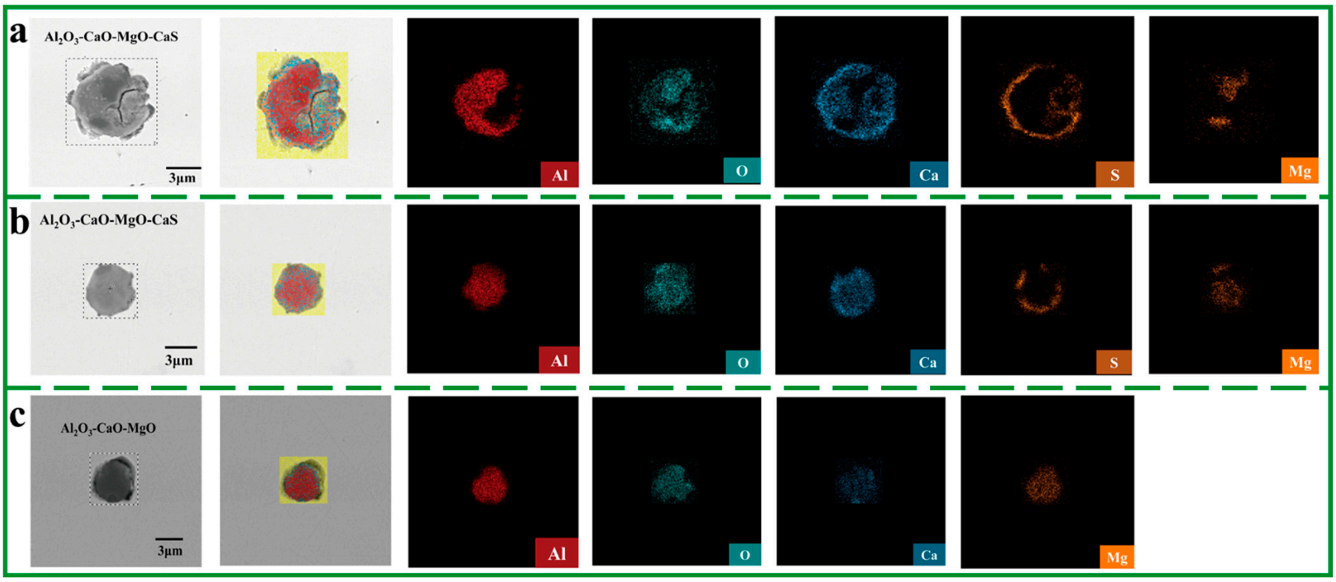

Figure 11. The element mapping of (**a**,**b**) Al_2O_3-CaO-MgO-CaS and (**c**) Al_2O_3-CaO-MgO.

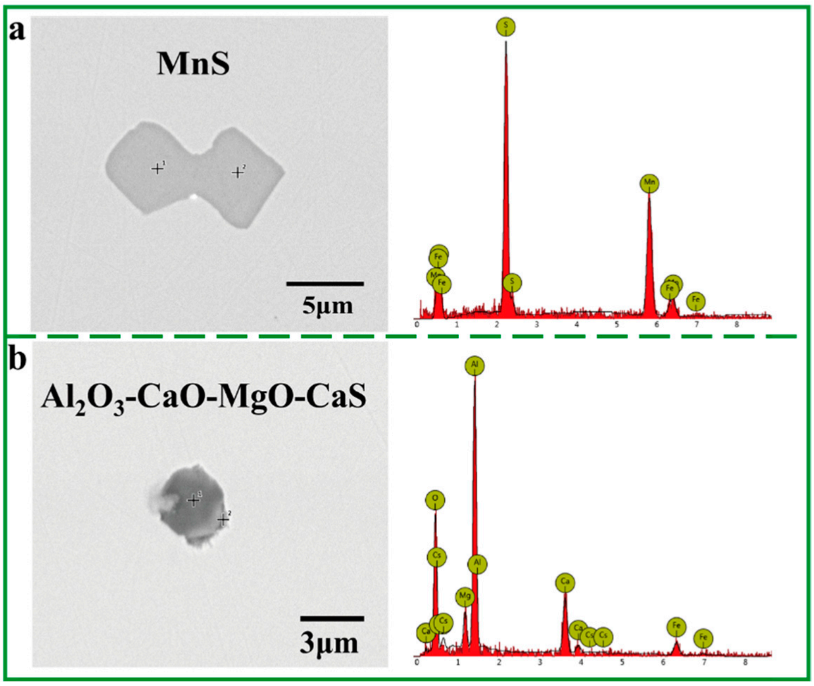

Figure 12. The composition of (**a**) MnS and (**b**) Al_2O_3-CaO-MgO-CaS inclusions.

42CrMo-S steel is deoxidized by aluminum throughout the process (Figure 1), so an Al_2O_3-MgO inclusion is formed in the molten steel after adding magnesium and aluminum deoxidizers. The Al_2O_3-MgO-CaO inclusion is formed after calcium treatment. After the S wire is fed, (Ca) and (S) combine to form CaS. Finally, the Al_2O_3-MgO-CaO-CaS inclusion (Figure 11) is formed, which is a complex inclusion containing calcium aluminate inside and enclosing the CaS layer outside. This kind of inclusion has high hardness and good toughness, and the anisotropy of steel can be improved.

The distribution of inclusions in the head billet with the growth of casting length is shown in Figure 13a. The size of large inclusions in the head billet performs a decreasing trend, and the distribution of inclusions in T1 and T2 is denser while the distribution of inclusions from T3 to T5 is more and more diffuse. The distribution of inclusions in the normal billet is also more diffuse, indicating that T3 to T5 can be used as the normal billet, confirming the conclusion obtained above. The distribution of inclusions in the tail billet with casting length growth is shown in Figure 13b. The inclusions in the tail billet primarily become diffuse and then become dense from W1 to W5, and the distribution of inclusions is similar to the normal billet.

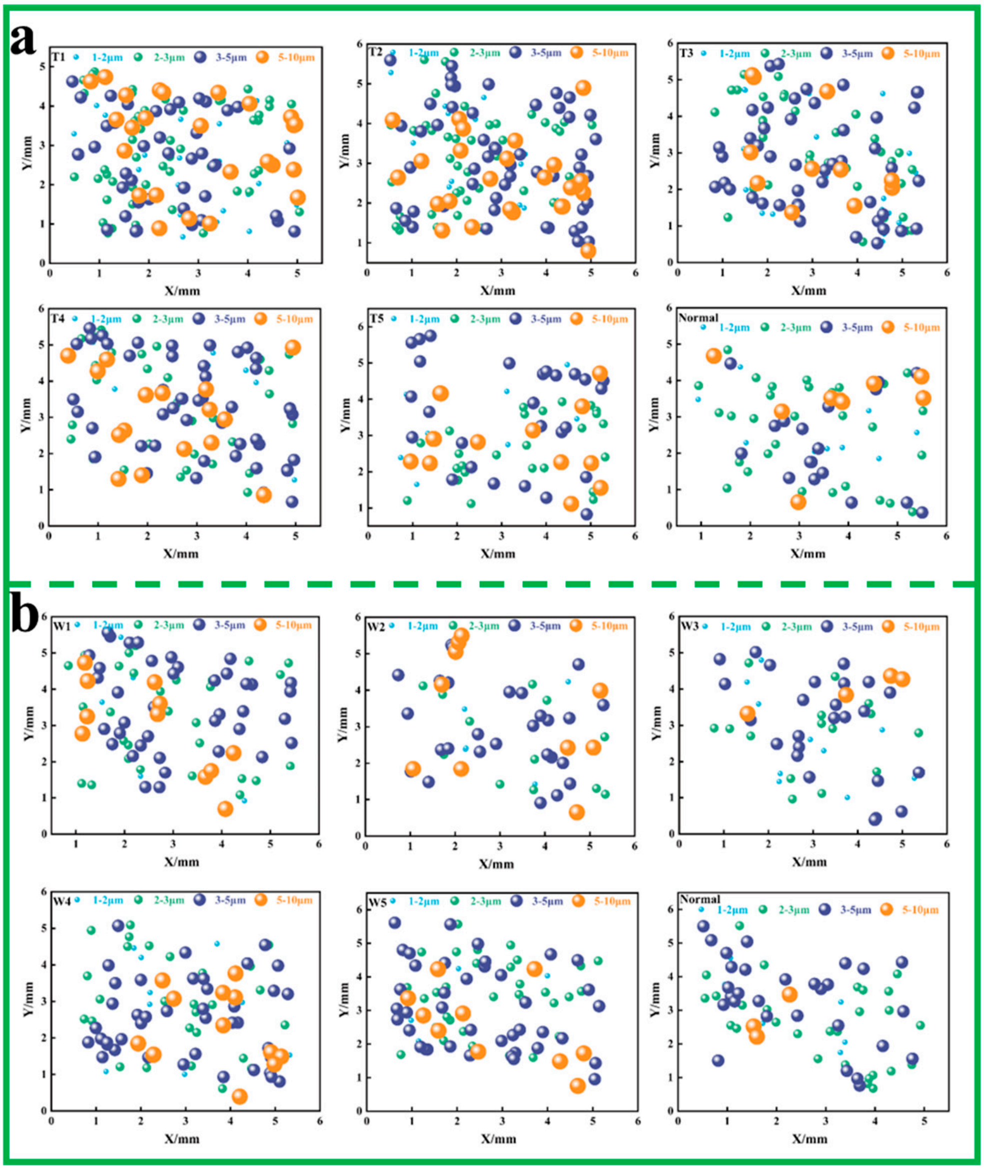

Figure 13. Distribution of (**a**) head billet and (**b**) tail billet inclusions.

The 42CrMo-S steel is deoxidized by aluminum throughout the process, so the Al_2O_3-MgO inclusion is formed in the molten steel after adding aluminum deoxidizers. The Al_2O_3-MgO-CaO inclusion is formed after calcium treatment and is used as the core for sulfide nucleation and precipitation [30]. After the S wire is fed, (Ca) and (S) combine to form CaS and finally form the Al_2O_3-MgO-CaO-CaS inclusions, which is a complex inclusion containing calcium aluminate inside and enclosing the CaS layer outside. This kind of inclusion has high hardness and good toughness, and the anisotropy of steel can be improved.

In this paper, the types of inclusions are studied, and its morphology can be subsequently analyzed in order to understand the morphology of different types of inclusions. The 2D morphology of the head and tail billet inclusions is analyzed. The inclusions can be analyzed in 3D by using small sample electrolysis. Three-dimensional morphology can have a more stereoscopic understanding of inclusions morphology. In future work, it can also study the refining slag composition changes, basicity, and phase diagrams and give the optimal range of refining slag composition to provide guidance for the field of actual production.

5. Conclusions

In this paper, variation in the oxygen and nitrogen content and the number, type, size, and distribution pattern of inclusions in the refining process and head and tail billets of 42CrMo-S steel are conducted. The following conclusions are obtained:

(1) The oxygen content in the refining process is well controlled, with 10.2 ppm at the end of LF slagging. The oxygen content is reduced to less than 10 ppm in the RH refining process, with 6.3 ppm at end-RH. The oxygen content in the rolled material is 7.2 ppm, which is lower than 15 ppm of the internal control requirement. There is a steady increase in the nitrogen content of the steel during smelting, where the N content is 65 ppm at end-RH.

(2) The inclusions in the molten steel are mainly pure Al_2O_3 upon arrival at LF. As the refining proceeds, the number of Al_2O_3 inclusions gradually decreases and is modified into inclusions with Mg-Al spinel-type inclusions, Al_2O_3-MgO-CaO inclusions, and some Al_2O_3-CaO inclusions. The feeding of the S wire promotes CaS generation and the number of CaS-type inclusions in the steel reaches the maximum. The percentage of inclusions that are less than 5 μm in the refining process (except end-RH) is kept above 90%, and the control of large inclusions is satisfactory.

(3) The total oxygen content is stabilized at 15 ppm from T3 to T5, and the number of inclusions in the normal billet is closest to the number of inclusions in T3, so it is recommended that the reasonable cut scrap length of the head billet is 0.3 m.

(4) The total oxygen content of the tail billet does not fluctuate much with the growth of casting length and is stable at about 15 ppm. Moreover, the number of inclusions in different sizes of W1 is closest to the normal billet, so it is recommended that the reasonable cut scrap length of the tail billet is 1 m.

Author Contributions: Methodology, M.W.; Validation, L.X.; Writing—original draft, B.W.; Writing—review & editing, L.X.; Funding acquisition, Y.B. All authors have read and agreed to the published version of the manuscript.

Funding: This research was funded by China Postdoctoral Science Foundation grant number 2023M730230; Fundamental Research Funds for the Central Universities grant number FRF-TP-22-053A1.

Data Availability Statement: Not applicable.

Conflicts of Interest: The authors declare that they have no known competing financial interests or personal relationships that could have appeared to influence the work reported in this paper.

References

1. Wang, Q.; He, Z.; Du, Z.; Wang, Q.; Dang, X.; Qi, Z.; Yang, C. Softening mechanisms and microstructure evolution of 42CrMo steel during hot compressive deformation. *J. Mater. Res. Technol.* **2023**, *23*, 5152–5163. [CrossRef]
2. Yang, Y.; Wei, X.; Long, Z.; Song, C.; Xie, C.; Lin, J. The Grey-Taguchi method analysis for processing parameters optimization and experimental assessment of 42CrMo steel treated by ultrasonic surface rolling. *J. Mater. Res. Technol.* **2023**, *23*, 6244–6261. [CrossRef]
3. Sui, G.; Wang, Z.; Fang, X.; Gao, G.; Zhao, C.; Guo, Y.; Song, Y.; Jiang, F. Ratchetting-fatigue behavior of a 42CrMo steel under near-yield mean stress. *Int. J. Mech. Sci.* **2023**, *247*, 108166. [CrossRef]
4. Fu, C.; Zhang, N.; He, G.; Jiang, B.; Liu, Y. Microstructural and finite element simulation analysis of the crack formed during heat treatment in the carburized 22CrMoH steel gear shaft. *Eng. Fail. Anal.* **2023**, *147*, 107165. [CrossRef]
5. Dai, Y.; Kang, L.; Han, S.; Li, Y.; Liu, Y.; Lei, S.; Wang, C. Surface Hardening Behavior of Advanced Gear Steel C61 by a Novel Solid-Solution Carburizing Process. *Metals* **2022**, *12*, 379. [CrossRef]
6. Han, X.; Chen, L.; Hu, X.; Hua, L.; Chai, F. Microstructure and mechanical property evolution mechanisms of 15Cr14Co12Mo5Ni2WA aviation gear steel during cold rotary forging. *J. Mater. Res. Technol.* **2023**, *24*, 3005–3022. [CrossRef]
7. Chen, Z.; Zhou, H.; Zhu, Z.; Xu, C.; Zhou, Y. Laser Cladding Remanufacturing of Aircraft Landing Gear Based on 30CrMnSiNi2A Steel. *Optik* **2023**, *283*, 170902. [CrossRef]

8. Sui, G.; Wang, Z.; Jiang, F.; Zhao, C.; Guo, Y.; Li, W. Fatigue crack growth behavior of 42CrMo high-strength steel with tempered sorbite/bainite microstructures: Roles of grain and constituent in microstructures. *Eng. Fract. Mech.* **2023**, *279*, 109051. [CrossRef]
9. Chen, M.-S.; Lin, Y.; Ma, X.-S. The kinetics of dynamic recrystallization of 42CrMo steel. *Mater. Sci. Eng. A* **2012**, *556*, 260–266. [CrossRef]
10. Huang, W.; Zhong, H.; Lei, L.; Fang, G. Microstructure and mechanical properties of multi-pass forged and annealed 42CrMo steel. *Mater. Sci. Eng. A* **2022**, *831*, 142191. [CrossRef]
11. Vijay Sekar, K.S.; Gobivel, K. Experimental and numerical investigations in the turning of 42CrMo alloy steel. *Mater. Today Proc.* **2023**, *in press*. [CrossRef]
12. Liu, X.; Yang, J.; Zhang, F.; Fu, X.; Li, H.; Yang, C. Experimental and DFT study on cerium inclusions in clean steels. *J. Rare Earths* **2020**, *39*, 477–486. [CrossRef]
13. Wagner, R.; Lehnert, R.; Storti, E.; Ditscherlein, L.; Schröder, C.; Dudczig, S.; Peuker, U.A.; Volkova, O.; Aneziris, C.G.; Biermann, H.; et al. Nanoindentation of alumina and multiphase inclusions in 42CrMo4 steel. *Mater. Charact.* **2022**, *193*, 112257. [CrossRef]
14. Wang, X.; Wu, Z.; Li, B.; Chen, W.; Zhang, J.; Mao, J. Inclusions modification by rare earth in steel and the resulting properties: A review. *J. Rare Earths* **2023**, *in press*. [CrossRef]
15. Gillner, K.; Henrich, M.; Münstermann, S. Numerical study of inclusion parameters and their influence on fatigue lifetime. *Int. J. Fatigue* **2018**, *111*, 70–80. [CrossRef]
16. Wang, Y.; Liao, S.; Pan, Z.; Jiang, S.; Fan, J.; Yu, S.; Xue, L.; Yang, J.; Ma, S.; Liu, T.; et al. Hydrogen sulfide alleviates particulate matter-induced emphysema and airway inflammation by suppressing ferroptosis. *Free Radic. Biol. Med.* **2022**, *186*, 1–16. [CrossRef] [PubMed]
17. Li, Y.; He, Y.; Ren, Z.; Bao, Y.; Wang, R. Comparative Study of the Cleanliness of Interstitial-Free Steel with Low and High Phosphorus Contents. *Steel Res. Int.* **2021**, *92*, 2000581. [CrossRef]
18. Wang, Y.; Bai, H.; Liu, C.; Zhang, H.; Ni, H.; Jönsson, P. Estimation of the probable maximum size of inclusions using statistics of extreme values and particle size distribution methods. *J. Mater. Res. Technol.* **2022**, *20*, 2454–2465. [CrossRef]
19. Wang, Y.N.; Bao, Y.P.; Wang, M.; Zhang, L.C. Precipitation and control of BN inclusions in 42CrMo steel and their effect on machinability. *Int. J. Miner. Metall. Mater.* **2013**, *20*, 842–849. [CrossRef]
20. Lin, C.-K.; Pan, Y.-C.; Su, Y.-H.F.; Lin, G.-R.; Hwang, W.-S.; Kuo, J.-C. Effects of Mg-Al-O-Mn-S inclusion on the nucleation of acicular ferrite in magnesium-containing low-carbon steel. *Mater. Charact.* **2018**, *141*, 318–327. [CrossRef]
21. Zhao, D.; Li, H.; Cui, Y.; Yang, J. Control of Inclusion Composition in Calcium Treated Aluminum Killed Steels. *ISIJ Int.* **2016**, *56*, 1181–1187. [CrossRef]
22. Yao, Z.; Ma, X.; Lyu, S. Phase equilibria of the Al_2O_3–CaO–SiO_2-(0%, 5%, 10%) MgO slag system for non-metallic inclusions control. *Calphad* **2020**, *72*, 102227. [CrossRef]
23. Su, L.; Xu, J.; Li, G.; Zhu, C. Influences of deoxidation and VOD slag on the behavior of inclusions in Fe–21Cr ferrite stainless steel. *J. Mater. Res. Technol.* **2021**, *15*, 1949–1958. [CrossRef]
24. Wang, Y.; Liu, C. Evolution and deformability of inclusions in Al-killed steel with rare earth-alkali metals (Ca or Mg) combined treatment. *J. Rare Earths* **2022**, *in press*. [CrossRef]
25. Wang, J.; Xue, P.; Zhang, L.; You, L.; Zhu, X.; Wang, S.; Zhong, Y.; Mao, X. Distribution behavior of inclusions in compact-strip-produced martensitic steel and its influence on mechanical properties. *J. Mater. Sci. Technol.* **2023**, *142*, 98–111. [CrossRef]
26. Wang, Y.; Sun, X.; Zhang, L.; Ren, Y. Effect of calcium treatment on inclusions in Si-Mn-killed 304 stainless steels. *J. Mater. Res. Technol.* **2020**, *9*, 11351–11360. [CrossRef]
27. Guo, Y.-T.; Wang, Q.; Chen, G.-J.; He, S.-P. Castability of aluminum- and sulfur-bearing free-cutting steel. *J. Iron Steel Res. Int.* **2015**, *22*, 87–92. [CrossRef]
28. Li, Z.; Liu, C.-J.; Sun, Q.; Jiang, M.-F. Effect of deoxidation process on distribution characteristics of inclusions in silicon steel slabs. *J. Iron Steel Res. Int.* **2015**, *22*, 104–110. [CrossRef]
29. Xing, L.; Bao, Y.; Wang, M. Evolution of inclusions in the whole process of GCr15 bearing steel. *Met. Res. Technol.* **2023**, *120*, 301. [CrossRef]
30. Su, L.; Tian, J.; Hu, S.; Lv, M.; Li, X.; Qu, T.; Wang, D.; Zhan, T. Effect of Ca/Mg on Distribution and Morphology of MnS Inclusions in 45MnVS Non-Quenched and Tempered Steel. *Metals* **2022**, *13*, 23. [CrossRef]